An efficient transient simulation procedure for the reliable estimation of draft tube losses in the hydraulic design process

IOP Conf. Series: Earth and Environmental Science **240** (2019) 072017 doi:10.1088/1755-1315/240/7/072017

An efficient transient simulation procedure for the reliable estimation of draft tube losses in the hydraulic design process

Paul Weber and Roland Jester-Zürker

Voith Hydro Holding GmbH & Co. KG, Alexanderstr. 11, 89522 Heidenheim, Germany

E-mail: paul.weber@voith.com, roland.jester-zuerker@voith.com

Abstract. Draft tube flow plays a significant role for the overall performance of a hydraulic machine and requires therefore special attention in the design process. However, as it is characterized by complex flow phenomena like swirl, adverse pressure gradients and flow separation, accurate predictions are challenging. Though the required technologies like transient simulation techniques and adequate turbulence modeling are available, it is especially the tremendous time consumption that renders the according analysis infeasible for the hydraulic design process.

In this contribution a new simulation methodology is presented that accelerates transient simulations in three ways. Firstly, the computational domain is significantly reduced by substituting the distributor with appropriate boundary conditions. Secondly, it is shown by a grid study that meshes with intermediate resolutions are to be favored over massively refined grids. And thirdly, a timestep study uncovers potential for increased step sizes. The proposed methodology is validated by comparison to PIV measurements performed by Frey et al. (IOP Conf. Ser.: Earth and Env. Sci. 49 082007), thus demonstrating that the developed workflow yields accurate and reliable results.

1. Introduction

The hydraulic development of modern hydro turbines is crucially dependent on numerical methods, whereby Computational Fluid Dynamics (CFD) in particular has evolved as the dominating analysis tool. It enables to identify and eliminate design deficiencies already in early stages, thus paving the way for sophisticated machine designs that are both robust and highly efficient. As a consequence, the margins for efficiency improvements shrink continually, which makes the pendulum swing back and necessitates analysis methods that provide even more accurate predictions.

In the design phase of hydraulic machines most of the simulations are by steady-state CFD, which yield reliable predictions within a short time frame. However, the reliability depends on the operating point and is only given for flow situations with a well-aligned flow structure and without transient large-scale phenomena. As the flow becomes increasingly more unstable, as it is for off-design conditions typically the case, the prediction quality worsens. In case of a reduced flow through a Francis turbine, for instance, the residual swirl causes a precessing part load vortex structure which has a dominating impact on the overall hydrodynamics in the draft tube [3]. Capturing this vortex is challenging which gives rise to widely different results.

During the last decade considerable effort was spent to investigate the draft tube hydrodynamics numerically, often with a focus on the part load vortex. Scherer et al. [12] performed transient simulations and compared the results to pressure measurements. Based on their findings they developed a turbine with 50 % reduced pressure pulsations. Ruprecht et al. [11] simulated the vortex rope with several turbulence models, proving the standard k-ε model and its two-scale version to be insufficient. For an adequate treatment of the inherent vortex instationarity the authors suggest employment of the Very Large Eddy Simulation. Vu et al. [13] also asserted the sensitivity regarding turbulence modeling, agreeing that the k-ε model is a poor choice for operating conditions away from the optimum. Though stationary simulations are not converging properly in such situations, smart averaging of the results can approximate the ones from transient simulations surprisingly well. Foroutan and Yavuzkurt [4] studied the relation of turbulence models, stationary and transient simulations. For stationary computations, the turbulence modeling was found to be of minor importance, whereas transient computations significantly improved with more sophisticated models like hybrid URANS/LES. Examining turbulence models as well, Agostini Neto et al. [1], compared k-ω SST and SAS models to LDA measurements. In addition to their finding that the transient SAS model outperforms other approaches, they discovered that refining a mesh has only marginal effects on the prediction accuracy. Besides others, the SAS has also been successfully used by Melot et al. [9], who analyzed pressure pulsations, and by Maddahian et al. [8], who focused on the vortex formation and movement.

The majority of the performed studies suggests that steady-state simulations are unreliable for part load operating conditions and that transient computations should be applied instead. But though transient methods have been developed and used in other areas for decades now, they are not applicable to the standard design process of water turbines yet. They are undoubtedly appealing due to their prediction capability, however, their tremendous time consumption renders their use impractical.

The focus of the present work is on techniques which reduce the computational costs of transient turbine simulations yet at the same time retain the accuracy, aiming to make transient simulations feasible for the time-constrained design process. This objective is achieved by reducing the computational domain, by limiting the mesh resolution and by increasing the timestep on the basis of a careful analysis. Using a Francis turbine with a specific speed of $n_q = 80$ as example, it is shown that the distributor can be excluded from the computational domain and that comparatively coarse spatial and temporal discretizations are sufficient. This is confirmed by comparison to detailed measurements by Frey et al. [5], showing that the proposed methodology is valid and applicable for industrial applications.

2. Numerical modeling

Aiming at the simulation of an operating point with part load vortex, the advice from the literature is followed and the turbulence is modeled via the SAS-SST approach. Besides a proper turbulence treatment, resolving a part load vortex requires a 360° modeling of the runner, since simulating a single channel with periodic boundary conditions cannot reproduce the required asymmetry. The inlet boundary conditions are obtained by a stationary simulation, which ensures a velocity profile featuring the characteristic wakes. This process is described in detail later on. Figure 1 (a) depicts the computational domain, which consists of runner and draft tube. Between the rotating (orange) and stationary domain a transient rotor stator interface is defined. The distance between interface and runner outlet is approximately 25 % of the runner diameter, whereby the stationary walls inside the rotating domain are modeled as counter-rotating boundaries. At the draft tube exit an extension with slip wall boundary conditions is added to avoid numerical disturbances in the flow regions of interest. At the domain outlet an opening boundary condition with average zero relative pressure is applied.

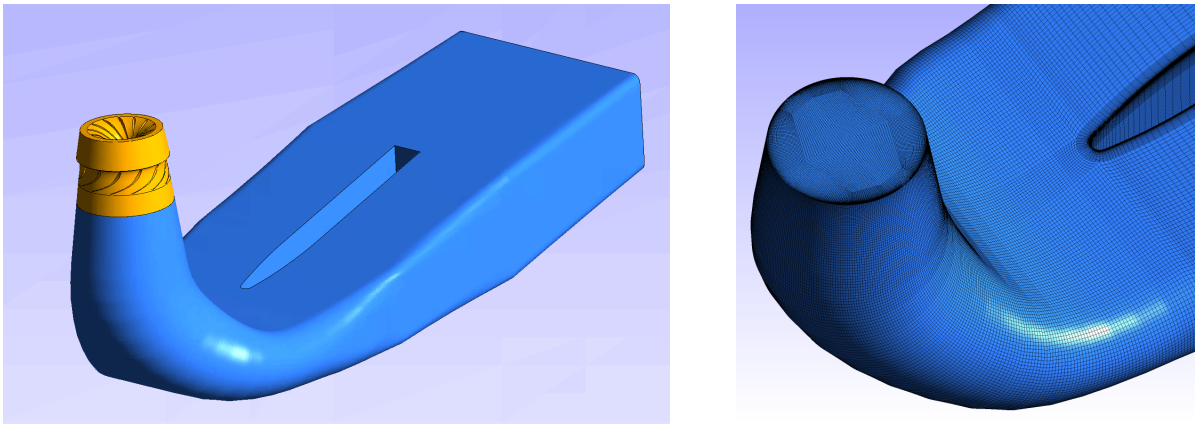

(a) Computational domain. (b) Draft tube mesh.

Figure 1. Computational domain and draft tube mesh of reference grid.

The geometry is discretized by a fully-structured multi-block mesh generated with an in-house code, a tool tailored to the specific peculiarities of hydro turbine geometries. All meshes of the grid study have identical blocking topologies, the only adjustments are by the number of points and point distributions of the individual blocks. In Figure 1 (b) the draft tube mesh used for reference is presented.

The numerical simulations were carried out with Ansys CFX 18.1.

3. A time-efficient yet accurate simulation methodology

The classical approach to transient turbine simulations includes three machine components: the draft tube and both a 360° distributor and rotor. The individual parts are meshed with a resolution common for steady-state simulations; the same holds true for the timestep. While this procedure produces reliable results it fails to integrate into the hydraulic design process because of its immense computational costs. Targeting a more sophisticated methodology that delivers results within days instead of weeks, there are three principle ways for improvement:

(i) Reducing the size of the computational domain
(ii) Reducing the grid resolution
(iii) Increasing the timestep

The approach is therefore to question the status quo of the standard workflow in terms of the domain size, grid resolution and timestep, and to ask which of them can be adapted without losing prediction accuracy.

3.1. Domain reduction

Given the confined machine geometry, the computational domain cannot be reduced by repositioning the boundaries. Instead, one has to remove entire machine components and integrate the information the components would add to the system in terms of boundary conditions. To simulate the turbine runner for instance, the spiral case is commonly modeled by an analytical flow description. If the interest is in the draft tube, one can proceed in a similar way and account for the influence of the distributor likewise, except that the flow structure at the runner inlet is far more complex and lacks an explicit mathematical expression. Instead, one can pre-compute the runner inflow conditions by means of a stationary simulation. That way the highly inhomogeneous flow at the wicket gate outlets are precisely captured. Having the velocity

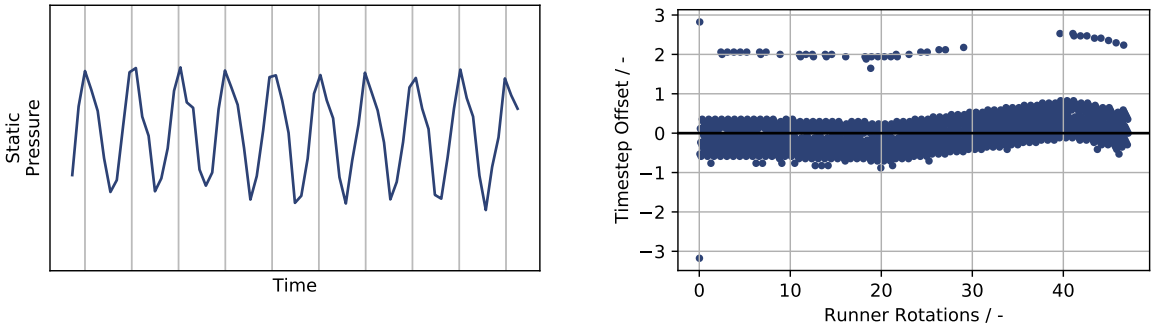

(a) Pressure oscillations.

(b) Timestep offsets of pressure peaks.

Figure 2. Oscillating pressure and timestep offsets due to gate passing shows correct implementation of counter-rotating runner inlet boundary conditions.

and turbulence fields determined, the distributor can be removed and the pre-calculated fields be applied as inlet boundary conditions for the rotor. One has therefore the following procedure:

(i) Make a steady-state simulation of the entire machine
(ii) Extract the velocity field and turbulence data at the distributor outlet
(iii) Remove the distributor from the simulation model
(iv) Apply the obtained boundary profiles as counter-rotating inflow fields of the rotor domain
(v) Perform the transient simulation for the reduced domain

This approach has multiple benefits. First, one avoids recomputing the low-influence temporal changes in the distributor. Second, one reduces the overall cell count by up to 30 %. And third, one eliminates the grid interface between the stationary distributor and the rotating runner. Compared to the approach by Melot et al. [9], who used a single-channel distributor, a full runner and the draft tube, the here proposed workflow requires even less computational resources. In total, the computational costs are reduced to roughly a third, and, if performed correctly, without deteriorating the numerical results.

3.1.1. Validation of the domain reduction Setting up the counter-rotating boundary condition has to be done with care since a wrong rotation direction or speed spoils the rotor-stator interaction and thus the entire simulation. A thorough validation of the physical interaction is therefore indispensable. To do so one monitors the pressure between guide vanes and runner blades in the rotating system and analyzes the static pressure oscillations. From the machine design and operation conditions one knows the gate passing frequencies, allowing to match the computed pressure peaks with the expected ones.

Plotting the monitored pressure and indicating the analytically expected peaks by a vertical line yields Figure 2 (a). The agreement of computed and expected pressure peaks is excellent, implying a correct relative velocity between boundary and rotor. The figure is however limited to a short timespan of not even half a runner rotation. While depicting the pressure evolution is intuitive and easy to interpret, this approach does not lend itself to longer time intervals involving several hundred pressure peaks. Hence, for monitoring over the entire simulation time a different representation is required.

The essential property of a computed pressure peak is how close it is to an expected peak. It is one number that characterizes the quality of each peak, namely, the time difference. Sorting all detected peaks on a time line with their time offsets on the y-axis yields a scatter plot as in

Figure 2 (b). Each point belongs to an algorithmically identified pressure peak, with the timestep offset being the time difference to the closest analytical peak, normalized by the timestep size. A point with an offset of 0.75 thus corresponds to a pressure peak that is 0.75 timesteps too early or too late. Looking at the figure, the offsets are consistently below 1, and, because the timestep is of integer type, are thus of the highest possible accuracy. The only exceptions are two points at the simulation start, as well as a line of samples with an offset of approximately 2. However, closer inspection reveals that those outliers are due to noisy pressure data and are therefore just false peak detections.

In total, Figure 2 confirms the matching of theoretical and simulated gate passings. The profile data from the stationary domain has been correctly used as counter-rotating inflow condition for the runner, i.e., the domain reduction has been successfully implemented.

3.2. Optimized grid resolution

Another approach for shortening simulation times is by choosing a grid resolution as coarse as possible but still fine enough to capture the necessary details. Once identified, the sweet spot cannot be directly transferred to other scenarios, however, a thorough grid study can reveal guiding information for related setups. As for the transient simulation of runner and draft tube, simulations with five subsequently refined meshes have been performed. In the following, the different grids are indicated by the coarsening exponent γ ranging from 0 to 4, where the according cell counts C_γ are

$$C_\gamma = 2^{-\gamma}\, C_0.$$

Here, C_0 denotes the cell count of the reference grid. Thus, for each coarsening step the amount of cells is halved. For $\gamma = 0$ the average y^+ value is 0.83; the coarser meshes have been generated without the $y^+ \leq 1$ constraint and have values of 34.5, 75.6 and 101, respectively. Each simulation has been carried out according to the above workflow for domain reduction and is analyzed regarding multiple aspects. After evaluating the losses for draft tube and runner, the numerically obtained velocities are compared to PIV measurements. The results indicate that beyond a critical resolution further cells are of limited use.

3.2.1. Component-wise losses At its core, the simulation pipeline is built to compute a single number that quantifies the machine. As the simulation has to be transient, time-local results have to be averaged over a sufficiently long timespan, yielding less volatile predictions the longer the simulated time.

Figure 3 depicts the time-averaged draft tube and runner losses over time for the five different grids calculated. The losses are plotted as relative delta to the final loss prediction by the finest grid,

$$\Delta\zeta_\gamma = \frac{\zeta_\gamma}{\bar{\zeta}_0} - 1,$$

whereby ζ_γ denotes the loss prediction by grid γ, and $\bar{\zeta}_0$ the time-averaged loss of the finest grid. All curves exhibit a falloff in the initialization phase, followed by an upwards trend till a plateau stage is reached. The initially strong oscillations introduced by the partload vortex are diminished over time, though some fluctuations remain. After around 30 runner rotations, all of the predictions are roughly in their final region, see Table 1 for the latest averages.

There is no unifying trend among the values the different simulations converge to. Despite the wide range of resolutions with up to 16 times finer grids, the predictions remain a) all within the same region and b) miss a general tendency. Framed by the two coarsest grids, the finer ones approach a loss delta of only 1 %. Refining the draft tube has in the present case therefore no interpretable advantage. Interestingly enough, the research by Devals et al. [2] yielded the exact opposite result, namely consistent accuracy improvements for finer meshes. However, there are

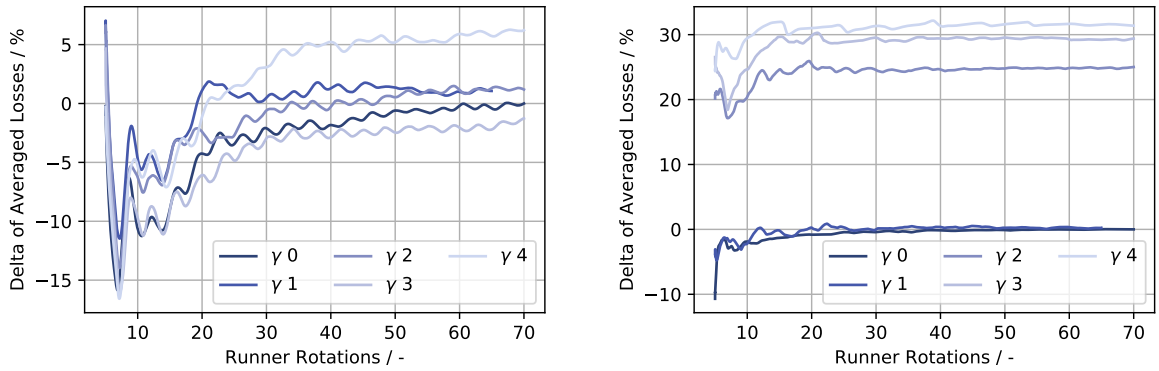

(a) Draft tube.

(b) Runner.

Figure 3. Development of time-averaged losses in machine components.

major differences in the simulation method, which is here transient and scale-adaptive opposed to stationary with RANS with k-ϵ closure, and also in the computational domain. Here, we employ a runner/draft tube configuration with non-averaged inflow data, the study of Devals et al. is restricted to the draft tube itself using an axisymmetric velocity profile as boundary condition. But probably more important than the differences in the techniques themselves is the interplay with the operating point. Having resolved the part load vortex, the flow characteristics are entirely different and possibly less sensitive to varying grid sizes. This is confirmed by the work of Agostini Neto et al. [1], who also investigated a part load operating point and found only negligible differences in the results of two differently refined meshes.

Considering the runner losses in Figure 3 (b), the behavior is substantially different. The coarsest mesh being 31 % off from the finest, the loss deltas consistently decrease with higher cell counts (cf. Table 1). In terms of monotonicity one has the ideal picture of steadily approximating a limit. In terms of absolute values one notices a huge jump between the $\gamma = 1$ and 2 grids, the gap is about 25 % of the predicted value. For the considered machine and operating point there has to be a hydrodynamical phenomenon that is unresolved in case of too low resolutions, but adequately captured once a certain resolution is reached.

3.2.2. Comparison of cone velocities to PIV measurements As reference for the comparison of velocities serve PIV measurements, taken in a plane between the runner trailing edges and the elbow entrance. The computed velocities are examined on (plane-) global and local levels.

γ	0	1	2	3	4
Draft Tube	0.00	1.07	1.18	-1.26	6.23
Runner	0.00	0.24	25.01	29.39	31.38

Table 1. Component-wise time-averaged delta losses in percent

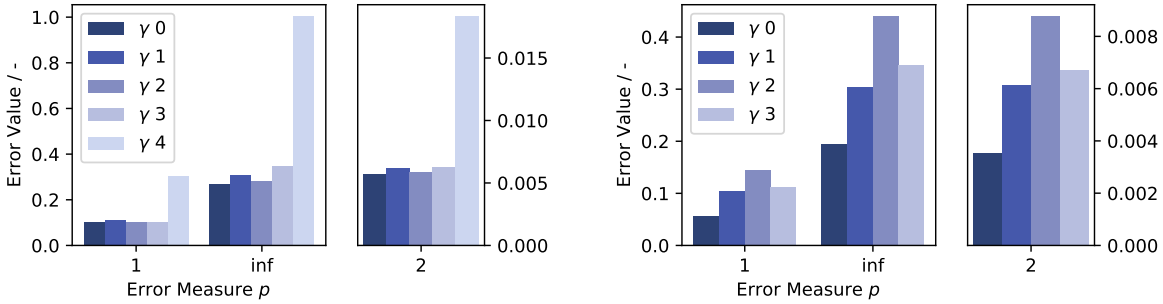

(a) Axial velocity component.

(b) Circumferential velocity component.

Figure 4. Global velocity errors in the cone measurement plane confirm negligible influence of grid resolution.

Global errors Figure 4 depicts the l_p-errors for the measured velocity components, axial and circumferential, defined as

$$l_p(\tilde{\boldsymbol{x}}; \boldsymbol{x}) = \begin{cases} \frac{1}{N} \left(\sum_i |x_i - \tilde{x}_i|^p\right)^{\frac{1}{p}}, & \text{if } p < \infty, \\ \max_i |x_i - \tilde{x}_i|, & \text{if } p = \infty. \end{cases}$$

Thereby denote $\boldsymbol{x}$ and $\tilde{\boldsymbol{x}}$ the measured and computed velocities with the individual values x_i and $\tilde{x}_i$, respectively, and N the number of entries. For the different values of p one has the arithmetic mean ($p = 1$), a RMS-related error ($p = 2$) and the maximal error ($p = \infty$).

Looking at the errors for the axial velocity in Figure 4 (a), there is little variation between the grids $\gamma = 0$ to 3. The predictions of the coarsest grid are entirely different, having errors 3 times as large. While the finer grids lack a trend as before, the coarsest grid breaks the pattern. However, the bad prediction quality is limited to small regions, because as seen before from Figure 3 the overall performance of the $\gamma = 4$ grid is without abnormality. As the remainder focuses on the measuring plane, and the data for the coarsest grid fails to add value to the analysis, it is omitted from now on.

Figure 4 (a) contains the errors for $p = 1$, 2 and ∞, whereby the l_2 errors are plotted separately because of their different order of magnitude. Except of minor differences, the shapes of the errors of identical p are similar. Irrespective of the measure the errors are almost constant. This homogeneity indicates consistency between the refinement levels in the sense that the individual discretizations are uniformly refined, successfully avoiding to favor one region over another.

For the errors in the circumferential velocities as shown in Figure 4 (b) the same holds true; all measures produce similar-looking shapes. The values are in the same order of magnitude as the axial errors, however, a trend is observable. Though not in a monotone manner, finer meshes lead to better results. Relative to $\gamma = 2$ the velocity errors drop more than 50 %, which is indeed visible in the velocity profiles discussed in the next section.

Local errors The most detailed comparison to measurement data is by direct investigation of the velocity field, which has additionally the charm to be intrinsically intuitive. Figure 5 depicts axial and circumferential velocities over the radius. Both plots are divided into two parts; the upper contains the velocities, the lower the offset to the measurements. The velocities are normalized by theoretical homogeneous velocity, $v_{\text{ref}} = \frac{Q}{A}$, where Q is the total volume flux and A the cone cross section in the measuring plane. The measurement data is plotted as dots.

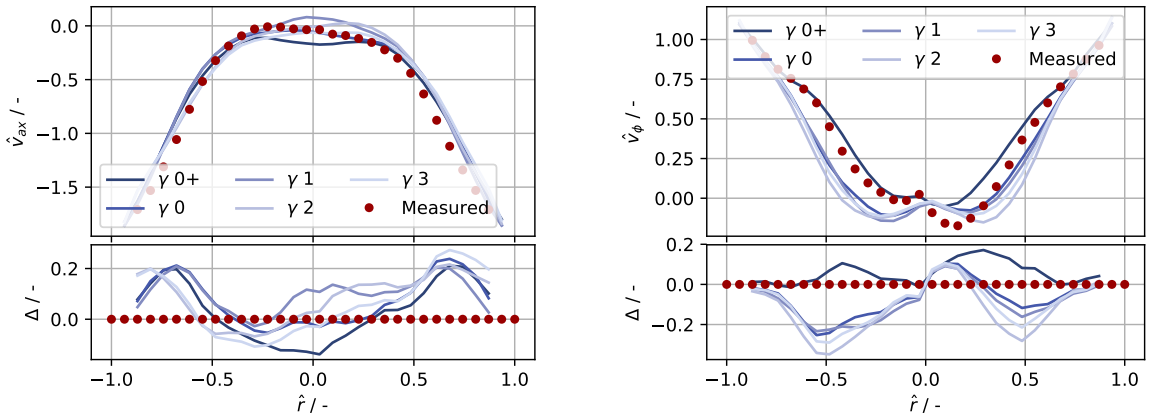

(a) Axial velocity over radius at $\phi = 78.75$.

(b) Circumferential velocity over radius at $\phi = 168.75$.

Figure 5. Axial and circumferential velocity components along a line in cone compared to PIV measurements. The circumferential velocity develops a trend for finer computational meshes.

The velocity components impress by their high accuracy for all of the four grids, in particular the left plot on the axial velocities. As expected from the global errors there is only a minimal difference between the individual grids. For the circumferential velocities, the overall agreement of the grids is slightly worse. While all predictions agree regarding the general shape, the finest grid is separate from the others and in the left half significantly closer to the measurements, which explains the error reduction seen in Figure 4 (b). In the right half, the prediction of the finest grid is however not superior, but because of the close approximation in the left half the measured asymmetry of the flow field is captured.

Interpreting the velocity field, the volume fluxes are high in the outer region, whereas towards the center the flow stagnates or turns into slight backflow. The circumferential component is likewise large at the boundaries, becoming smaller in the proximity of the center. At $\hat{r} \approx 0.15$ there is even a counter-rotating flow due to the developed rope vortex, which is, under time-averaging, significantly less pronounced on the opposing side. As all of the simulations fail to capture this behavior accurately, it is probably triggered by the spiral case and stay vane/wicket gate flow, which have been modeled and thus lack some nuances.

3.2.3. Remarks on grid-refinement The performed grid study has now been discussed for component-wise losses in runner and draft tube, and for the individual velocity components in the first draft tube section, the cone. On the component level, it is the runner that benefits substantially from grid refinements, while the draft tube losses are mesh-independent. In the cone, which is spatially connecting runner and draft tube, one has also in terms of convergence a transitional behavior. Axial velocities are widely unaffected by varying mesh resolutions, circumferential velocities in contrast benefit from refinements and show a mostly continuous improvement. In both cases the trends are the more pronounced the more global the perspective is. This has important implications for draft tube simulations and their evaluations:

- If the interest is in global losses, the prediction quality is for comparatively coarse grids already resolution-independent. Further refinements are superfluous.
- If the interest is in local quantities like velocities, grid refinements have a perceptible but limited effect. Furthermore, improvements can be restricted to an individual velocity component.

Though the second implication is in a way unsatisfactory, the first is indeed beneficial for the present purpose of efficiently predicting the draft tube efficiency; higher grid resolutions fail to yield more accurate results, which frees from the ubiquitous demand for further refinement and the accompanying prolonged computation times. However, it has to be noted that the obtained results may be specific to the considered operation point. For instance, reducing the flow volume further and thus going deeper into part load, the vortex rope recedes, the flow characteristics change and the results may become sensitive to meshing details.

3.3. Optimized timestep

Analogously to the mesh resolution, the optimal timestep is as large as possible but small enough to resolve the necessary details. To assess the timestep-sensitivity of the results a series of simulations with different step sizes has been run. Starting with the step size as used for the grid study, t_0, subsequent timesteps are defined by

$$t_i = 2^i \, t_0$$

for $i = 1, \ldots, 4$. Figures 6 (a) and 6 (b) depict the time-averaged losses in draft tube and runner, similar to Figures 3 (a) and 3 (b). As before, both losses exhibit an initialization and plateau phase, the latter becoming increasingly stable. Comparing the grid- and timestep-study plots for draft tube losses, it is remarkable that there is no major difference, neither in the general shape nor in the relation of the individual curves. On closer inspection one notices the smaller variance in the losses of the timestep study, only 4 % instead of 7 %, and that the result of the smallest timestep can be seen as an outlier. The runner losses, in contrast, are easily distinguishable. While there is a clear and consistent improvement for finer meshes, smaller timesteps have little impact on the accuracy. Decreasing from around 30 % by higher spatial resolution, temporal resolution influences the accuracy only in a range of 5 %. Furthermore, there is no trend and no significant drop.

It is important to notice that for both components, runner and draft tube, the results stay at the same level of accuracy even for the largest timestep, being 16 times larger than the initial. This indicates a huge potential which should be investigated in more detail.

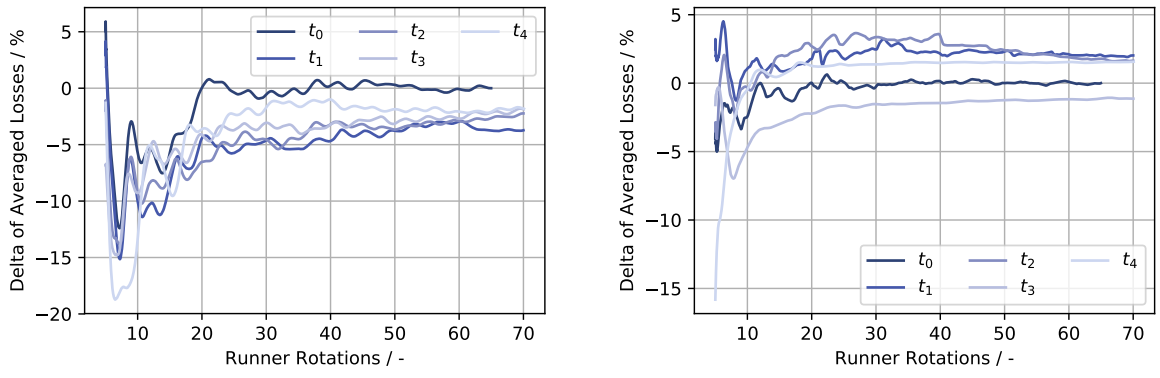

(a) Draft tube.

(b) Runner.

Figure 6. Development of time-averaged losses in machine components for simulations with increasing timestep.

4. Summary

The proposed methodology for time-efficient transient simulations has as its key components the domain reduction by substituting the distributor domain by pre-simulated boundary data, and the appropriate choice of mesh resolution and timestep, taking into account the early grid- and timestep-independence of the draft tube. The former reduces the demand of computational time in multiple ways, most prominently by cutting down the total cell count by up to 30 %, the latter allows for spatial and temporal discretizations significantly coarser than one would intuitively use. Though one cannot formulate a guideline on the optimal discretization, the results indicate a huge potential that can be tapped on a case-to-case basis. Quantitative rules however require more research.

For the proposed methodology, each of the key aspects has been studied in detail: the correct application of the stator domain substitution by monitoring the gate passing frequencies, the influence of mesh refinements by error analysis and measurement comparisons, and the sensitivity towards the timestep by a series of simulations. The entirety of the obtained results asserts the validity of the proposed methodology.

Acknowledgment

We would like to thank the anonymous reviewers for their detailed inspection and remarks.

References

[1] Agostini Neto A D, Jester-Zuerker R, Jung A and Maiwald M 2012 Evaluation of a Francis turbine draft tube flow at part load using hybrid RANS-LES turbulence modeling *IOP Conf. Ser.: Earth and Environmental Science* **15** 062010
[2] Devals C, Vu T C, Zhang Y, Dompierre J and Guibualt F 2016 Mesh convergence study for hydraulic turbine draft-tube *IOP Conf. Ser.: Earth and Environmental Science* **49** 082021
[3] Dörfler P, Sick M, Coutu A 2013 *Flow-Induced Pulsation and Vibration in Hydroelectric Machinery* (London: Springer)
[4] Foroutan H and Yavuzkurt S 2012 Simulation of flow in a simplified draft tube: turbulence closure considerations *IOP Conf. Series: Earth and Environmental Science* **15** 022020
[5] Frey A, Kirschner O, Riedelbauch S, Jester-Zuerker R and Jung A 2016 Reference measurements on a francis model turbine with 2D laser-doppler-anemometry *IOP Conf. Ser.: Earth and Environmental Science* **49** 082007
[6] Krappel T, Riedelbauch S, Jester-Zuerker R, Jung A, Flurl B, Unger F and Galpin P 2016 Turbulence resolving flow simulations of a francis turbine in part load using highly parallel CFD simulations *IOP Conf. Ser.: Earth and Environmental Science* **49** 062014
[7] Menter F 2011 Best Practice: Scale-Resolving Simulations in ANSYS CFD
[8] Maddahian R, Cervantes M J and Sotoudeh N 2016 Numerical investigation of the flow structure in a Kaplan draft tube at part load *IOP Conf. Ser.: Earth and Environmental Science* **49** 022008
[9] Melot M, Nennemann B and Désy N 2014 Draft tube pressure pulsation predictions in Francis turbines with transient Computational Fluid Dynamics methodology *IOP Conf. Ser.: Earth and Environmental Science* **22** 032002
[10] Mulu BG, Cervantes MJ, Devals C, Vu TC and Guibault F 2015 Simulation-based investigation of unsteady flow in near-hub region of a Kaplan turbine with experimental comparison *Eng. App. of Computational Fluid Mechanics* **9:1** 139–156
[11] Ruprecht A, Helmrich T, Aschenbrenner T and Scherer T 2002 Simulation of vortex rope in a turbine draft tube *Proc. of the 21st IAHR Symp. on Hydraulic Machinery and Systems* Lausanne
[12] Scherer T, Faigle P and Aschenbrenner T 2002 Experimental analysis and numerical calculation of the rotating vortex rope in a draft tube at part load *Proc. of the 21st IAHR Symp. on Hydraulic Machinery and Systems* Lausanne
[13] Vu T C, Devals C, Zhang Y, Nennemann B and Guibault T 2011 Steady and unsteady flow computation in an elbow draft tube with experimental validation *International Journal of Fluid Machinery and Systems* **4** 1